Microchimica Acta (2024) 191:359
https://doi.org/10.1007/s00604-024-06413-1

REVIEW ARTICLE

From theory to practice: understanding the challenges in the implementation of electrogenerated chemiluminescence for analytical applications

Gabriele Giagu[1] · Alessandro Fracassa[1] · Andrea Fiorani[2] · Elena Villani[3] · Francesco Paolucci[1] · Giovanni Valenti[1] · Alessandra Zanut[4]

Received: 20 March 2024 / Accepted: 10 May 2024 / Published online: 31 May 2024

Abstract

Electrogenerated chemiluminescence (ECL) stands out as a remarkable phenomenon of light emission at electrodes initiated by electrogenerated species in solution. Characterized by its exceptional sensitivity and minimal background optical signals, ECL finds applications across diverse domains, including biosensing, imaging, and various analytical applications. This review aims to serve as a comprehensive guide to the utilization of ECL in analytical applications. Beginning with a brief exposition on the theory at the basis of ECL generation, we elucidate the diverse systems employed to initiate ECL. Furthermore, we delineate the principal systems utilized for ECL generation in analytical contexts, elucidating both advantages and challenges inherent to their use. Additionally, we provide an overview of different electrode materials and novel ECL-based protocols tailored for analytical purposes, with a specific emphasis on biosensing applications.

Keywords Electrochemiluminescence · Biosensor · Electrochemistry · Sensors

Introduction

Electrogenerated chemiluminescence (ECL) is a phenomenon of light emission at electrodes in electrochemical cells caused by energetic electron transfer (redox) reactions of electrogenerated species in solution [1, 2]. The peculiarity of this technique lies in the generation of reactive intermediate species at the electrode's surface that react with one another, resulting in an excited state capable of emitting light [3]. This way of generating excited states in ECL makes it an extraordinarily versatile technique ensuring remarkable sensitivity and nearly absent background optical signals. This is attributed to the activation of luminophores through electrochemical processes rather than external light stimuli.

In addition to that, by tuning the applied voltage or current, the rate of electron transfer reactions can be precisely controlled, thereby affecting the kinetics of the overall reaction. This capacity for fine-tuning enables the optimization of reaction conditions, leading to improved reproducibility, efficiency, and selectivity in the ECL process.

ECL benefits also from a diverse array of molecules that can act as luminophores, along with compatible coreactants. This extensive selection ensures optimal compatibility across various systems, including aqueous solutions. Moreover, the integration of electrochemiluminescent labels with biological molecules enables the development of highly sensitive and specific biosensors allowing researchers to design assays tailored to specific applications, thereby enhancing the precision and efficiency in detecting and analyzing biomolecular interactions [4–6].

For instance, in biosensing, ECL is used for detecting and quantifying a wide range of biomolecules with outstanding sensitivity and specificity, making it useful for applications

✉ Giovanni Valenti
g.valenti@unibo.it

✉ Alessandra Zanut
alessandra.zanut@unipd.it

[1] Department of Chemistry Giacomo Ciamician, University of Bologna, via Selmi 2, Bologna 40126, Italy

[2] Department of Chemistry, Keio University, 3-14-1 Hiyoshi, Yokohama 223-8522, Japan

[3] Department of Chemical Science and Engineering, School of Materials and Chemical Technology, Tokyo Institute of Technology, Yokohama 226-8502, Japan

[4] Present Address: Department of Chemical Sciences, University of Padova, via Marzolo 1, Padua 35131, Italy

in medical diagnostics, environmental monitoring, and drug development. On the other hand, in imaging applications, ECL emerges as a formidable tool for visualizing biological processes at both cellular and molecular scales. This capability provides researchers with a powerful tool to investigate physiological mechanisms and understand disease pathology [7–10].

In ECL, the excited state capable of emitting light is generated through a combination of electrochemical and chemical reactions which can be classified in two main categories: annihilation mechanism [11] and coreactant mechanism [12, 13].

The annihilation mechanism involves an electron transfer reaction between high energetic radical anion and cation of the luminophore, which are generated electrochemically at the electrode, with consequent population of the excited state. This is generally achieved by fast switching the electrode potential from oxidation to reduction currents (or vice versa), with radical annihilation taking place inside the diffusion layer [14].

The coreactant mechanism involves a chemical reaction that occurs after the electrogeneration of the radicals and before the electron transfer to excite the luminophore. The coreactant is a sacrificial molecule that conversely to the luminophore is not recovered after the light emission. It is, in fact, this irreversible chemical reaction of the coreactant (after its oxidation or reduction) that promotes the transformation of the coreactant into a high energetic radical specie [12, 15]. In the following sections, we aim to give useful information on the application of ECL in analytical settings. In particular, we will provide an overview of the theoretical foundations of ECL generation, and we will outline the key systems employed for ECL generation in analytical scenarios, discussing both their advantages and challenges.

Energy requirements for light emission in ECL

The main focus of an ECL reaction centers around the generation of an excited species capable of emitting light, as previously noted.

In the annihilation reaction, the energy required for the formation of the excited state originates from the interaction between the two radical ions, which are produced by the alternating switch of the potential of the electrode between positive and negative values [16].

ECL emission can only occur if the combined energy of these two species exceeds that of the excited state [17] (Eq. 1).

$$\Delta G = E^{\circ}_{red} - E^{\circ}_{ox} + E_{es} \quad (1)$$

In this context, ΔG is the Gibbs free energy change for the annihilation reaction, E^{0}_{red} and E^{0}_{ox} are the standard potentials of the luminophore for reduction and oxidation, respectively, and E_{es} is the energy difference between the emitting excited state and the ground state of the luminophore [4].

Conversely, in a reaction involving a coreactant, the excited state arises from species generated via an electron transfer reaction between the luminophore (or one of its derivatives) and a species produced following the oxidation or reduction of the coreactant at the electrode surface [18]. For the coreactant pathway, the ΔG is as reported in Eq. 2 or 3 depending on the oxidized or reduced form of the luminophore, respectively:

$$\Delta G = E^{\circ}_{Cor} - E^{\circ}_{Ox} + E_{es} \quad (2)$$

or

$$\Delta G = E^{\circ}_{Red} - E^{\circ}_{Cor} + E_{es} \quad (3)$$

These equations exemplify a reaction where the ECL emission occurs through coreactant and luminophore electron transfer reaction. In this scenario, a highly reactive radical species originated from the coreactant generates the excited state, rather than the electro-reduced (or oxidized) form of the luminophore. Importantly, as Eqs. 2 and 3 suggest, successful light emission relies on the effective energy transfer facilitated by electron transfer ($\Delta G < 0$). This implies a tight link between the electron transfer energy and the luminophore's emission energy. Essentially, when the emission energy is high, it becomes essential to have a coreactant capable of providing the necessary energy [19, 20].

Such boundary conditions have been defined as ECL "wall of energy sufficiency," and it could be implied to predict whether a luminophore is theoretically capable of emitting light.

Stringer et al. provide a compelling example of this study [21]. They compared various metal complexes as potential luminophores in the coreactant ECL system with TPrA through the catalytic route. Their analysis relied on a "wall of energy sufficiency" plot (Fig. 1) which correlates the oxidation potential of each metal complex with its emission wavelength, where each point represents a potential luminophore. The dotted line indicates the "wall of energy sufficiency" for the TPrA system.

This scheme emphasizes the role of energy requirements to obtain a specific emission wavelength. A favorable luminophore must have an oxidation potential positive enough to enable efficient electron transfer between the HOMO state of TPrA and the LUMO state of the luminophore (Fig. 2).

The Marcus-Hush theory helps to explain why a more positive ΔG value favors the reaction leading to the excited state (inverted region) over the reaction leading to ground state products (normal region), based on kinetic aspects [22, 23].

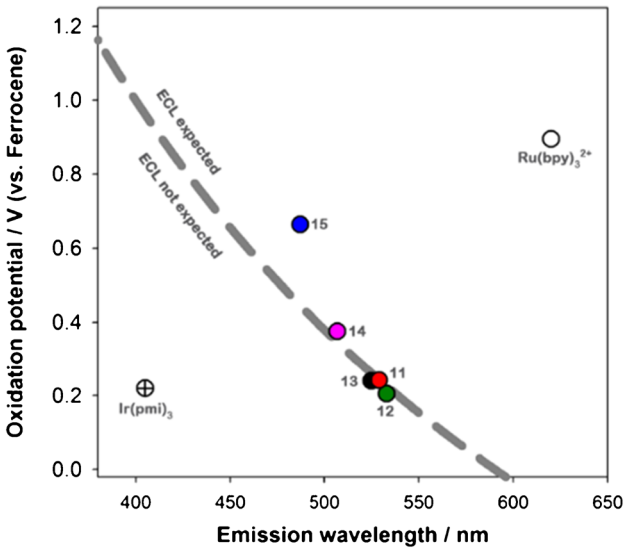

Fig. 1 This plot allows to visualize the "wall of energy sufficiency" for a TPrA system; each point represents a luminophore; luminophores above the dotted line are expected to emit light after electron transfer reaction with TPrA•; the ones below are expected to not emit light. Numbers 11–15 indicate the different $Ir(ppy)_2$ (C^C:) complexes tested. Adapted with permission from [21], Copyright (2014) American Chemical Society

When considering TPrA for ECL signal generation in a heterogeneous system (where the luminophore is fixed, as we will explore further), it is important to understand its mechanism introduced by Bard and his colleagues [12].

This mechanism differs in that the luminophore itself does not undergo an electrochemical reaction. Instead, TPrA acts as the sole species undergoing oxidation, forming the $TPrA^{\bullet+}$ radical cation. This radical quickly decomposes into the $TPrA^{\bullet}$ radical, which then reduces the luminophore. The resulting reduced luminophore can subsequently react with the $TPrA^{\bullet+}$ radical cation, leading to the generation of the excited state.

The energy involved in this heterogeneous reaction can be expressed as:

$$\Delta G = E^{\circ}_{Red} - E^{\circ}\left(TPrA^{\bullet+}\right) + E_{es} \tag{4}$$

This statement necessitates a critical consideration which involve an additional "energy barrier" that behaves similarly to the wall of energy (Fig. 3). In this case, for efficient electron transfer to populate the luminophore's LUMO (lowest unoccupied molecular orbital), the reduction potential (E°_{Red}) must be sufficiently negative. This ensures that the energy transferred from $TPrA^{\bullet+}$ to the luminophore is sufficient to overcome the energy gap between its ground and

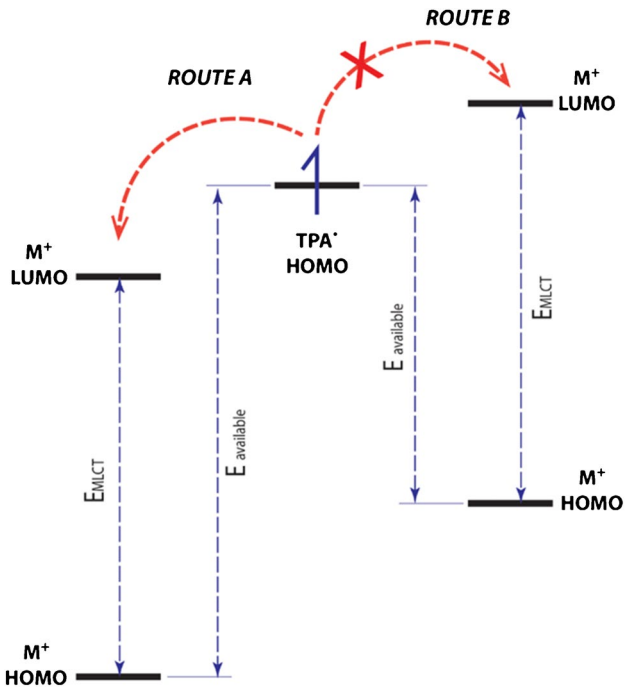

Fig. 2 Schematic representation of the ET reaction between $TPrA^{\bullet}$ and the luminophore for energy sufficient ET reaction for the population of the excited state (pathway A) and for non-sufficient ET reactions (pathway B). Adapted with permission from [21], Copyright (2014) American Chemical Society

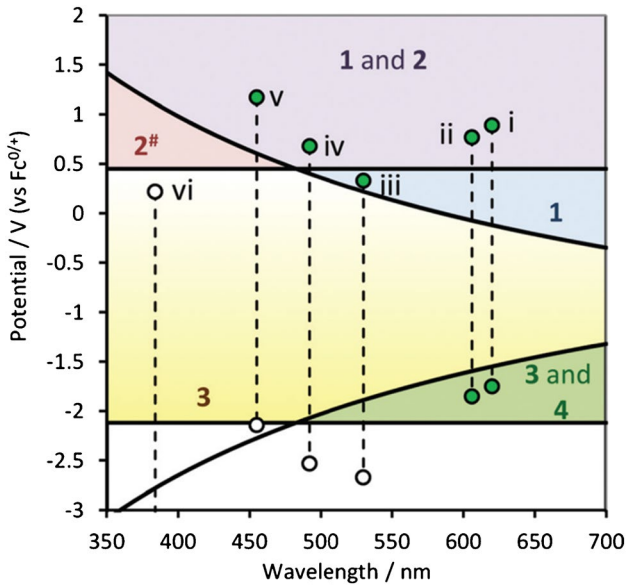

Fig. 3 Complete "wall of energy sufficiency" plot representation for complexes in a TPrA coreactant system showing the energy requirements for the different reaction pathways between the luminophore and the coreactant. This diagram depicts the energy requirements for various metal complexes, considering both their redox potentials and emission wavelengths. The numbers within the zones indicate which of the four TPrA reaction pathways are available for each complex based on its energetic positioning. Adapted with permission from [24], Copyright (2016) American Chemical Society

excited states. Essentially, a "favorable" energy landscape is required for successful light emission in this heterogeneous pathway [24–26].

ECL systems

ECL systems can be classified in several ways, for example based on (i) the luminophore [27], (ii) the coreactant [28], and (iii) the reaction mechanism that occurs between the two. Here, annihilation ECL will not be described as it is not relevant for analytical applications [6], although it holds important theoretical and mechanistic aspects [29].

Concerning the luminophores, there are inorganic complexes [3], mainly of Ru(II) [30] or Ir(III) [31, 32], luminol [33, 34], organic molecules (polycyclic aromatic hydrocarbons, BODIPY, fluorene, and spirobifluorene) [35, 36], carbon nanomaterials (carbon dots and graphitic carbon nitride) [37], semiconducting nanocrystals (NCs) and quantum dots (QDs) [38–42], and gold (Au) nanocluster [43].

However, among all the luminophores available, commercial applications of ECL exploit only ruthenium complexes, although iridium is gaining more attention for its promising higher photoluminescence and ECL efficiency than ruthenium [44]. Inorganic complexes offer a wide range of possible functionalization, are water soluble although iridium complexes require careful design to be made soluble while retaining efficient coreactant ECL [31], and can be synthetized homogeneously and precisely at the molecular level. Organic molecules have generally low or no water solubility; therefore, the conjugation synthesis to the biological receptor is complicated, or it requires expensive (cost and workup) modification of the luminophore. Nanomaterials are difficult to be produced in a standardized form to obtain the accuracy and reproducible results essential for applications actually reached in ECL analyzers.

In the group of coreactants, it is possible to find amines, the most efficient and used of those is tri-*n*-propylamine (TPrA), and oxalate for "oxidative-reduction" ECL mechanism (oxidation reaction), while persulfate, hydrogen peroxide, and benzoyl peroxide are suitable for

$$Ru(bpy)_3^{2+} \longrightarrow Ru(bpy)_3^{3+} + e^-$$
$$Ru(bpy)_3^{3+} + C_2O_4^{2-} \longrightarrow Ru(bpy)_3^{2+} + CO_2 + CO_2^{\bullet -}$$
$$Ru(bpy)_3^{3+} + CO_2^{\bullet -} \longrightarrow Ru(bpy)_3^{2+*} + CO_2$$
$$Ru(bpy)_3^{2+*} \longrightarrow Ru(bpy)_3^{2+} + h\nu$$

Scheme 1 ECL mechanism of oxalate and $Ru(bpy)_3^{2+}$

"reductive-oxidation" ECL mechanism (reduction reaction). Other coreactants exist, namely amine-related coreactants (amino acids, peptides, nucleic acid, NADH, alkaloids, pharmaceuticals, pesticides, hydrazine), organic acids, and alcohols, although the ECL signal can be considerably low. However, these molecules can be detected directly by acting both as coreactant and analyte [45].

Generally, the luminophore reacts with the coreactant, and it is regenerated after the light emission, except for luminol that is converted to an unreactive compound, 3-aminophthalate dianion [33]. Therefore, a useful classification of the ECL systems can be done based on the reaction mechanism that is peculiar of each coreactant. In the following section, the most important ECL mechanisms are described, providing their possible application in sensor development.

ECL mechanism by "oxidative-reduction"

This category comprises the coreactants that after oxidation form a high energetic radical that reduces the luminophore, such as oxalate and amines.

Oxalate was the first coreactant developed for aqueous solution reacting with $Ru(bpy)_3^{2+}$ [46], and for its detection in synthetic urine [47], as reported in Scheme 1.

The mechanism with TPrA is more complex and offers a wider applicability making it the only available to develop commercial instruments for clinical analysis. Beside the first described "oxidative-reduction" mechanism (Scheme 2), a mechanism that involves exclusively TPrA oxidation (Scheme 3) and a catalytic mechanism (Scheme 4) occur. In

Scheme 2 ECL "oxidative-reduction" mechanism of TPrA and $Ru(bpy)_3^{2+}$

$$TPrAH^+ \rightleftarrows TPrA + H^+$$
$$TPrA \rightleftarrows TPrA^{\bullet +} + e^-$$
$$TPrA^{\bullet +} \rightleftarrows TPrA^{\bullet} + H^+$$
$$Ru(bpy)_3^{2+} \longrightarrow Ru(bpy)_3^{3+} + e^-$$
$$Ru(bpy)_3^{3+} + TPrA^{\bullet} \longrightarrow Ru(bpy)_3^{2+*} + Pr_2N^+CHCH_2CH_3$$
$$Ru(bpy)_3^{2+*} \longrightarrow Ru(bpy)_3^{2+} + h\nu$$

Scheme 3 Heterogeneous ECL mechanism of TPrA and $Ru(bpy)_3^{2+}$

$$TPrAH^+ \rightleftarrows TPrA + H^+$$

$$TPrA \rightleftarrows TPrA^{\bullet+} + e^-$$

$$TPrA^{\bullet+} \rightleftarrows TPrA^{\bullet} + H^+$$

$$Ru(bpy)_3^{2+} + TPrA^{\bullet} \longrightarrow Ru(bpy)_3^{+} + Pr_2N^+CHCH_2CH_3$$

$$Ru(bpy)_3^{+} + TPrA^{\bullet+} \longrightarrow Ru(bpy)_3^{2+*} + TPrA$$

$$Ru(bpy)_3^{2+*} \longrightarrow Ru(bpy)_3^{2+} + h\nu$$

addition, annihilation between $Ru(bpy)_3^{3+}$ and $Ru(bpy)_3^{+}$ is theoretically possible in presence of TPrA [12].

Scheme 2 reports the first mechanism ever investigated with TPrA in aqueous solution (Fig. 4A) [48] which opened the application to clinical analysis and its commercial development [49]. Only few years later, the real mechanism responsible of the ECL emission in clinical analyzer was presented in a seminal paper from the Bard group [12] that has been demonstrated to involve only TPrA oxidation (Fig. 4B), while direct oxidation of $Ru(bpy)_3^{2+}$ was not necessary (Scheme 3).

The nomenclature "heterogeneous" comes directly from the application in the ECL analyzers where the $Ru(bpy)_3^{2+}$ is immobilized on microbeads or directly onto the electrode [3, 6, 15], meaning that it is not free to diffuse because belonging on a different phase (Scheme 3, Fig. 4B), in contrast with homogeneous case where both $Ru(bpy)_3^{2+}$ and TPrA are freely to diffuse in solution (Scheme 2, Fig. 4A).

The difference in the ECL mechanisms is highlighted in the different optimal pH value for the highest ECL emission (Fig. 5).

In fact, the reaction rate of the overall ECL mechanism is affected by the TPrA radical cation deprotonation to form the TPrA radical which is a function of the pH. Faster deprotonation in high pH increases the rate of mechanism 2 (Fig. 4A), while in low pH, the slower deprotonation enables the heterogeneous ECL mechanism 3 to be quantitatively relevant for the signal emission [52].

Beside the pH effect, the effect of amine radical cation deprotonation was clearly evident with the use of

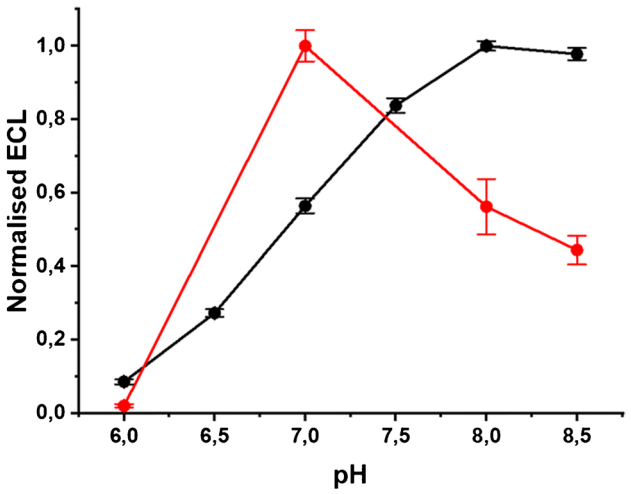

Fig. 5 Normalized ECL as a function of pH: $Ru(bpy)_3^{2+}$ free diffusing in solution (black), and $Ru(bpy)_3^{2+}$ labeled on 2.8-μm beads deposited on the electrode (red). Adapted with permission from [51], Copyright (2023) Royal Society of Chemistry

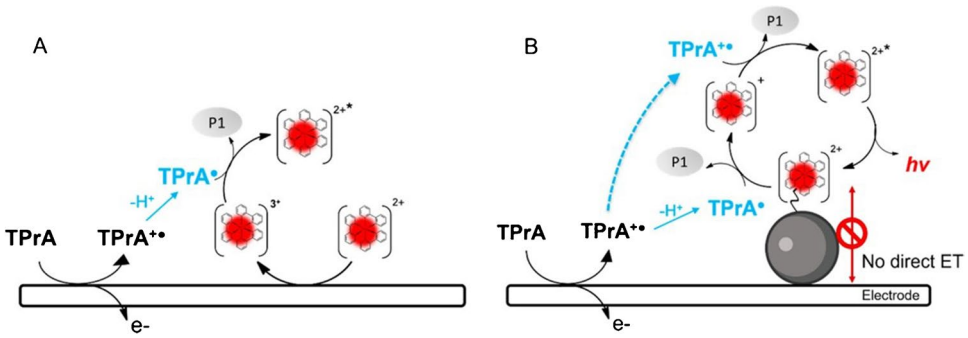

Fig. 4 Schematic representation of electrogenerated chemiluminescence mechanism involving TPrA and $Ru(bpy)_3^{2+}$: (**a**) homogeneous, where both coreactant and luminophore can be oxidized at the electrode surface; (**b**) heterogeneous where only the coreactant is oxidized. Adapted with permission from [50], Copyright (2022) American Chemical Society

Scheme 4 Catalytic ECL mechanism of TPrA and $Ru(bpy)_3^{2+}$

$$TPrAH^+ \rightleftarrows TPrA + H^+$$

$$Ru(bpy)_3^{2+} \longrightarrow Ru(bpy)_3^{3+} + e^-$$

$$TPrA + Ru(bpy)_3^{3+} \longrightarrow Ru(bpy)_3^{2+} + TPrA^{\bullet+}$$

$$TPrA^{\bullet+} \rightleftarrows TPrA^{\bullet} + H^+$$

$$Ru(bpy)_3^{3+} + TPrA^{\bullet} \longrightarrow Ru(bpy)_3^{2+*} + Pr_2N^+CHCH_2CH_3$$

$$Ru(bpy)_3^{2+*} \longrightarrow Ru(bpy)_3^{2+} + h\nu$$

2-(dibutylamino)ethanol (DBAE), in comparison with TPrA. The faster deprotonation enables high ECL signal for the mechanism 2 [53], but the emission is almost suppressed for heterogeneous ECL mechanism 3 when used with microbeads (Fig. 4B) [8].

The last mechanism that is possible to occur with the $Ru(bpy)_3^{2+}$/TPrA system is the catalytic mechanism, where the freely diffusing $Ru(bpy)_3^{3+}$ can oxidize the TPrA in solution as represented in Scheme 4.

This mechanism is generally observable at high $Ru(bpy)_3^{2+}$ concentration (hundreds µM to mM) [54], barely showing any practical interest for analytical purpose. However, recent investigations of homogeneous oxidation of TPrA by a freely diffusing Ir complex demonstrated that this strategy can increase the ECL signal from a microbeads immunoassay, i.e., heterogeneous system by a "redox mediated" pathway (Fig. 6) [55, 56]. The Ir(III) complex oxidized at the electrode to produce Ir(II) can oxidize the TPrA, which result in the formation of $TPrA^{\bullet}$, and in addition, it reacts with $Ru(bpy)_3^{+}$ to generate the excited state of $Ru(bpy)_3^{2+}$ with the overall effect of increasing the ECL signal up to 107%.

ECL mechanism by "reductive-oxidation"

This category comprises the coreactants that after reduction form a high energetic radical that oxidize the luminophore, mainly peroxides such as persulfate [13, 57, 58], hydrogen peroxide [59], and benzoyl peroxide [60].

All these coreactants follow the same reaction pathway, as illustrated for peroxydisulfate in Scheme 5.

The striking difference between $S_2O_8^{2-}$ and TPrA is that an heterogeneous mechanism is not possible and the reduction of the $Ru(bpy)_3^{2+}$ to $Ru(bpy)_3^{+}$ is essential. This has been demonstrated experimentally by labeling $Ru(bpy)_3^{2+}$ on microbeads, and the imaging analysis by a microscope did not reveal any ECL emission when the $S_2O_8^{2-}$ was the coreactant [61]. This further confirms the great importance of using TPrA for the ECL imaging of cells or large biological entities [62–64].

ECL from luminol

Luminol is an organic molecule which application in ECL is directly taken from chemiluminescence (CL) [65, 66].

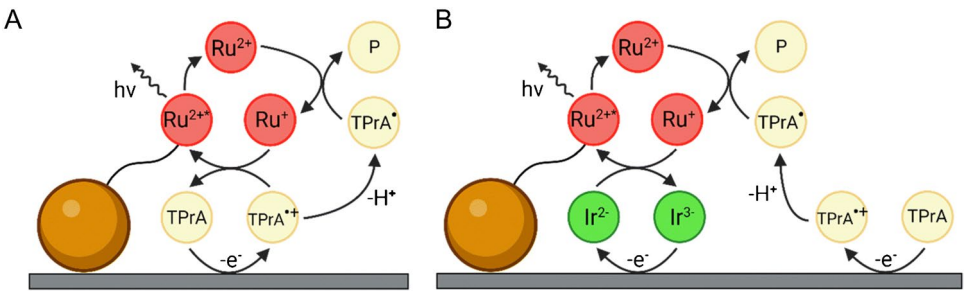

Fig. 6 Schematics of heterogeneous bead-based immunoassay: conventional ECL pathway (**a**) and the enhanced "redox mediated" pathway (**b**). The magnetic microbead is represented by the orange sphere while the $[Ru(bpy)_3]^{2+}$ luminophore and the $[Ir(sppy)_3]^{3-}$ complex are labeled as Ru^{2+} and Ir^{3-}, respectively. Adapted with permission from [56], Copyright (2024) Royal Society of Chemistry

Scheme 5 ECL "reductive-oxidation" mechanism of $S_2O_8^{2-}$ and $Ru(bpy)_3^{2+}$

$$Ru(bpy)_3^{2+} + e^- \longrightarrow Ru(bpy)_3^{+}$$

$$S_2O_8^{2-} + e^- \longrightarrow SO_4^{\bullet -} + SO_4^{2-}$$

$$Ru(bpy)_3^{+} + S_2O_8^{2-} \longrightarrow Ru(bpy)_3^{2+} + SO_4^{\bullet -} + SO_4^{2-}$$

$$Ru(bpy)_3^{+} + SO_4^{\bullet -} \longrightarrow Ru(bpy)_3^{2+*} + SO_4^{2-}$$

$$Ru(bpy)_3^{2+*} \longrightarrow Ru(bpy)_3^{2+} + h\nu$$

Luminol has a characteristic chemiluminescence emission centered at 425 nm, from the 3-aminophthalatedianion (3AP) excited state, though depending on the solvent can emit light in a range from around 424 to 510 nm, with ECL centered at 440 nm [33, 67]. Luminol reacts with H_2O_2 to generate CL in the presence of a suitable catalyst (peroxidase or metal ions), while in ECL, the electrochemical stimulus triggers the light emission. For this reason, luminol is used in combination with oxidases which produce H_2O_2 in analytical applications. The mechanism proceeds by luminol oxidation at the electrode and following reaction with H_2O_2. The adduct releases a N_2 molecule to form the 3AP in the excited state that emits light (Scheme 6). Depending on the electrode material, solvent, and pH, the ECL emission from luminol is observed generally in the potential range between 0.3 and 0.5 V (vs. Ag/AgCl) [68–70].

In conclusion, we have to distinguish between sensor applications and ECL investigation on mechanisms and signal enhancement. If the target is the development of a sensor for a specific analyte, there is no doubt that the couple $Ru(bpy)_3^{2+}$/TPrA offers superior advantages in terms of ECL intensity, high reproducibility, simplicity, and the opportunity to use the heterogeneous ECL approach to implement a real sensing device. On the other hand, still the $Ru(bpy)_3^{2+}$/TPrA ECL mechanism needs further investigation toward fundamental understanding [15, 52], and in particular, to increase the ECL signal intensity [54, 55]. Moreover, other new ECL systems can be introduced [35, 71], in particular,

$$L \longrightarrow L^{\bullet +} + e^-$$

$$L^{\bullet +} \longrightarrow +L^{\bullet} + H^+$$

$$L^{\bullet} + H_2O_2 \longrightarrow 3AP^* + N_2$$

$$3AP^* \longrightarrow 3AP + h\nu$$

Scheme 6 Simplified reaction mechanism for ECL of luminol (L) with H_2O_2

concerning the luminophore, but these have to demonstrate true advantages when compared with the $Ru(bpy)_3^{2+}$/TPrA ECL system.

Electrode materials

Electrode materials for ECL does not differ from general electroanalytical techniques, although some particular attention has to be taken when the electrode material affects the ECL mechanisms, to match it with the ECL system of interest [72].

Noble metals: platinum and gold

Pt and Au electrodes are widely used in electrochemistry, as well as in ECL, in particular, for organic solvents and aprotic conditions and for the characterization of new luminophores, for example. This condition enables a potential window of about 3 V, enough to explore a wide range of annihilation mechanisms. Metals can have high purity (up to 99.99%); the shape is highly reproducible and the ductility allows the fabrication of electrodes with different dimensions (diameter from cm to μm). For example, with ultramicroelectrodes, the adverse effects of ohmic drop and cell time constant on establishing electrode potential, which originates from the fast potential switch in annihilation ECL, can be minimized. Another advantage of metal electrodes is their superior resistance to fouling when compared to glassy carbon.

Some drawbacks arise when metal electrodes are employed in aqueous solution, a general environment for sensing applications. The small overpotential for hydrogen or oxygen evolution reaction makes these reactions to compete with luminophore or coreactant electrochemical reactions.

Concerning the use of TPrA, its oxidation corresponds with the generation of an oxide layer on the electrode surface (0.2~1.4 V vs. SCE) that prevents almost completely the TPrA oxidation reducing the heterogeneous electron

transfer reaction. This results in serious quenching of the ECL signal. Au oxide formation is approximately 400 mV more positive than Pt oxide that gives Au a 10 times higher ECL emission compared to Pt (Fig. 7) [73].

Generally, the addition of surfactants, also alkanethiols in case of Au, could alleviate this problem by the formation of a hydrophobic layer on the electrode surface that reduces the generation of the oxide and increases the heterogeneous electron transfer of TPrA oxidation [74]. Another drawback encountered with noble metal electrodes can be the adsorption of intermediates originated from the coreactant oxidation that leads to poisoning of the metallic electrode surface. Therefore, either surfactants are used or not, the surface of metal electrodes requires a cleaning procedure (mechanical or electrochemical) after the ECL measurement to restore its initial state.

Gold electrodes were initially employed in the first commercially available ECL instrument (Origen I analyzer) introduced by IGEN International in 1994 [48, 49]. However, in contemporary technology for immunoassay

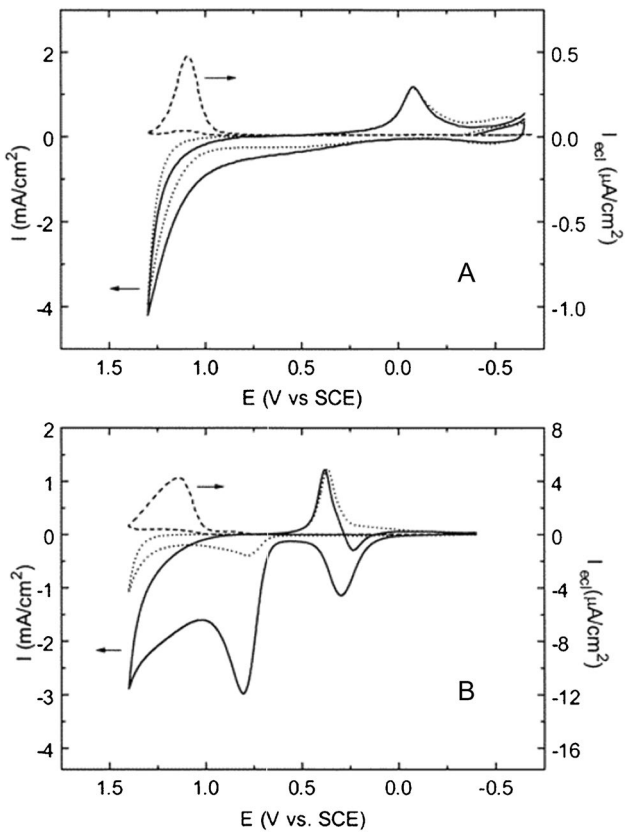

Fig. 7 Cyclic voltammogram and ECL curve at (**a**) platinum and (**b**) gold electrodes in 0.15 M phosphate buffer solutions (pH 7.5) containing 100 mM TPrA and 1 μM $Ru(bpy)_3^{2+}$. The dotted line represents data in the absence of both $Ru(bpy)_3^{2+}$ and TPrA. Potential scan rate, 0.1 V s^{-1}. Adapted with permission from [73], Copyright (2000) American Chemical Society

detection, Roche Diagnostics utilizes Pt instead [75]. This is mainly due to the lower propensity of Pt to form metal oxides and its easier electrochemical cleaning process [44].

Carbon-based electrodes

The first difference for these electrodes comes with the carbon hybridization. Generally, carbon electrodes are based on carbon black, carbon nanotubes, graphene, graphite, and glassy carbon, therefore sp^2 carbon. However, diamond (sp^3 carbon) electrodes are also employed in electrochemistry, and ECL as well, which will be discussed in a following section. Carbon electrodes show a fast kinetics of TPrA heterogeneous electron transfer reaction, and a sluggish kinetic for hydrogen and oxygen evolution, if compared to metal electrodes [76]. This makes carbon electrodes particularly suitable for ECL generation in aqueous electrolyte, and biosensors development, although the physical stability restricts the application to disposable platforms. This was excellently demonstrated by Meso Scale Discovery with the ECL analyzer based on multiarray technology where the platform for the ECL immunoassay (screen-printed carbon ink electrodes) resembles the ELISA method, where the recognition element is bound on the bottom of a well microtiter plates, and a sandwich immunoassay is formed by a secondary antibody labeled with the luminophore [6].

When compared to Au and Pt, glassy carbon showed 10 times and 100 times higher ECL emission, respectively (Fig. 8) [73].

In analogy with metal electrodes, glassy carbon requires a cleaning procedure (mechanical or electrochemical) after the ECL measurement to restore its initial state, because anodic oxidation during ECL generation and adsorption of intermediates lead to signal decrease [77]. In addition to glassy carbon, other carbon allotropes have been used for ECL, namely carbon nanotubes and graphene which generally require a substrate that serves as support [37]. These carbon materials also permit to prepare optically transparent electrodes for special applications, such as imaging, biosensors, or spectroscopy [62, 78–80].

Carbon nanomaterials not only act as electrode material but can be scaffolds to bind the recognition unit of biosensors, for example antibodies [81] or enzymes [34, 37]. Nevertheless, the main disadvantage of carbon electrodes can be the quality of the carbon structures. In fact, sp^3 carbon or defects in the sp^2 carbon structure could cause generation of unspecific signal that increases the background.

Although not strictly carbon electrodes, conducting polymers can be used for ECL. For example, poly(3,4-ethylenedioxythiophene) (PEDOT) and polypyrrole (PPy) films, and their composites, have been used with the luminol/H_2O_2 system for electrical property characterization of polymers by ECL imaging [69, 82, 83].

A particular carbon allotrope which is diamond is an intrinsic semiconductor with an indirect band gap of 5.47 eV [84].

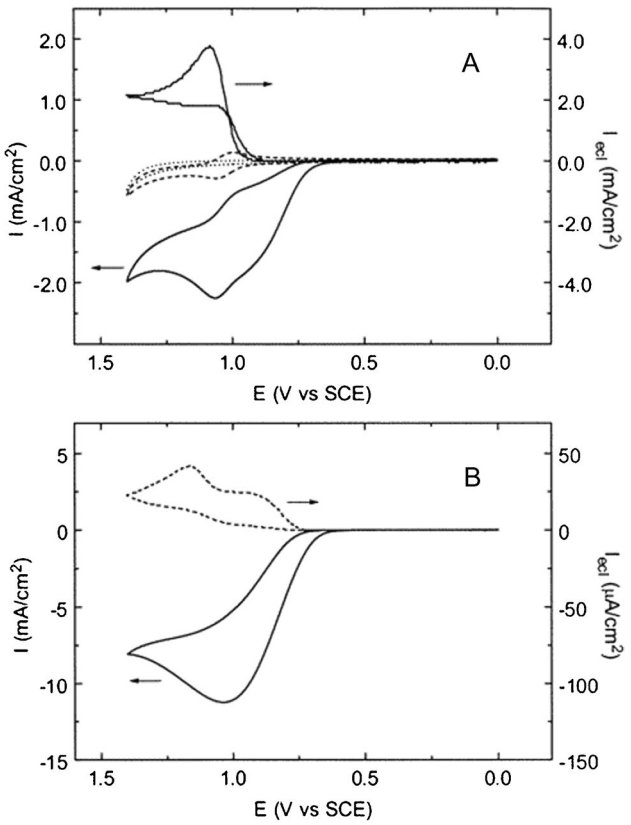

Fig. 8 (**a**) Cyclic voltammograms and ECL curve of 1 mM $Ru(bpy)_3^{2+}$ at a glassy carbon electrode in 0.15 M phosphate buffer solution (pH 7.5) in the presence (solid line) and absence (dashed line) of 10 mM TPrA. The dotted line represents data in the absence of both $Ru(bpy)_3^{2+}$ and TPrA. (**b**) Cyclic voltammogram and ECL curve at a glassy carbon electrode in 0.15 M phosphate buffer solution (pH 7.5) containing 100 mM TPrA and 1 μM $Ru(bpy)_3^{2+}$. Potential scan rate, 0.1 V s^{-1}. Adapted with permission from [73], Copyright (2000) American Chemical Society

To acquire the metallic conductivity necessary for electrochemistry, it is generally doped with boron at concentration around or higher than 10^{20} [B] cm^{-3} [85]. The electrochemistry of boron-doped diamond (BDD) has been established with application in chemical and biochemical sensing, environmental remediation, electrosynthesis, electrocatalysis, and energy storage and conversion [86], and recently, BDD has also been applied successfully to ECL [51]. Well-known characteristics include wide potential window in aqueous electrolyte (low catalytic activity for oxygen and hydrogen evolution reaction), low capacitive current, and physical and chemical stability.

ECL at BDD electrodes has been evaluated for the $Ru(bpy)_3^{2+}/S_2O_8^{2-}$ system where it showed higher emission than glassy carbon thanks to the low activity for hydrogen evolution [58]. For the $Ru(bpy)_3^{2+}$/TPrA systems, BDD showed higher emission in the heterogeneous system with microbeads compared to conditions mimicking the commercial immunoassay with Pt electrode (Fig. 9) [87].

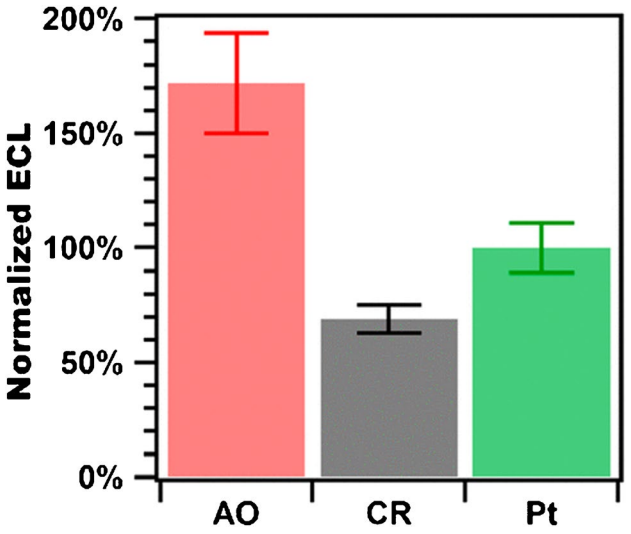

Fig. 9 Integrated ECL from $Ru(bpy)_3^{2+}$-labeled beads for anodic-oxidized (AO) BDD (red), cathodic-reduced (CR) BDD (gray), and Pt (green) electrodes. Adapted with permission from [87], Copyright (2022) American Chemical Society

The peculiar properties of BDD enabled to produce directly in situ the coreactant for the $Ru(bpy)_3^{2+}$ from sulfate or carbonate oxidation which generates $S_2O_8^{2-}$ or H_2O_2, respectively, for the "reductive-oxidation" ECL mechanism [88, 89]. The generation of the H_2O_2 coreactant directly in situ from carbonate oxidation was also reported for luminol ECL [33].

Generally, optimal boron doping level is around 1% of B/C ratio ($\approx 2\times10^{21}$ [B] cm^{-3}) for most of the common ECL systems [90].

Transparent electrodes

These electrodes find applications in combination with microscopy to image processes limited to the surface proximity, particularly for imaging of biological samples. Generally, two types of electrodes are available: glass/metal oxides (indium-doped tin oxide or fluorine-doped tin oxide) and carbon (nanotubes or graphene) on glass or polymer support. However, the electrochemistry of these two types of electrode is quite different, for example, the TPrA oxidation reaction rate on a carbon nanotubes electrode is about 30 times faster than on indium-doped tin oxide electrode, with an estimated heterogeneous electron transfer constant of 2.6×10^{-2} cm s^{-1} and 8×10^{-4} cm s^{-1}, respectively [78].

Paper-based microfluidic and screen-printed electrodes

Microfluidic paper-based analytical devices (mPADs) represent a class of materials that can be successfully coupled with ECL detection [91]. Inkjet printing technology can

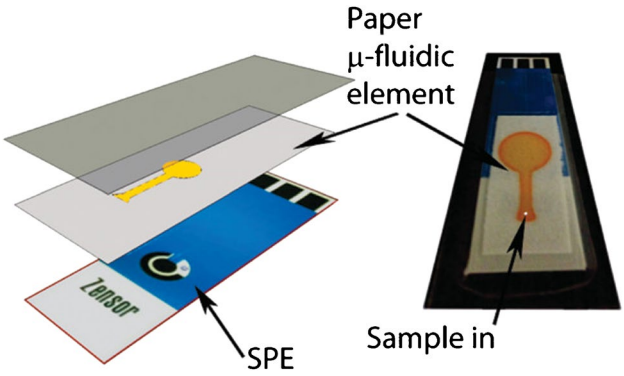

Fig. 10 Example of coupling paper-based microfluidic and screen-printed electrode to realize an analytical device. Adapted with permission from ref [92], Copyright (2011) American Chemical Society

be employed to fabricate paper microfluidic substrates, or alternatively using the strip-based rapid test, that in combination with screen-printed electrodes create a simple, easy to use, and disposable sensors. Moreover, the ECL signal can be detected by a smartphone camera to develop a portable device (Fig. 10) [92, 93].

ECL protocols

In recent years, the research of advanced analytical techniques has been triggered by the need for sensitive detection methods in various fields, particularly in strategies for biomarker detection. Consequently, a lot of effort has been dedicated to the development of new ECL-based protocols for the accurate determination of specific analytes through immunoassays, enzyme-based assays, and other methodologies, further harnessing the potential of ECL in modern analytical chemistry.

Luminophore conjugation

The transition metal complex $Ru(bpy)_3^{2+}$ is one of the most luminophore used in ECL, renowned for its widespread utilization as a probe. $Ru(bpy)_3^{2+}$ /TPrA systems react effectively and emit light in aqueous medium at room temperature (~25 °C) and at the proper pH range (see Fig. 5) in the presence of dissolved oxygen and other impurities [94]. $Ru(bpy)_3^{2+}$ can function as a reporter molecule through its ability to form conjugates with reactive groups present within biomolecules. Derivatives of the metal complex containing functional groups facilitating conjugation are employed for this purpose enabling the coupling with amino groups in proteins, peptides, ligands, and synthetic oligonucleotides. For instance, antibodies can be effectively labeled by covalently attaching the amino group in lysine to a $Ru(bpy)_3^{2+}$ -NHS ester, elucidating its applicability in immunoassays and beyond (Fig. 11) [95]. Moreover, the synthesis, labeling, and bioanalytical applications of this tris(2,2′-bipyridyl) ruthenium(II)-based ECL probe demonstrate its versatility and significance in modern analytical chemistry [94, 95, 96, 97, 98].

On the other hand, luminol is the most used organic ECL luminophores, featuring a low excitation potential and high ECL efficiency across both aqueous and solid phases [70, 94, 96]. Luminol is widely used in immunoassays, small molecule detection, and enzyme activity analyses. Its versatility is also given by the presence of an active amino group on its aromatic ring, facilitating facile coupling to other materials, particularly biomacromolecules, via covalent bonds preserving the stability of ECL signals and enhancing the accuracy of detection systems. Other luminol derivatives with different chemical functionalities, introduced onto the aromatic ring, were investigating to further enhance the ECL efficiency and improve the physicochemical properties of luminol-based assays (Fig. 11) [97]. For example, by adding a hydrophilic carboxylate group to the benzene ring of luminol, the resulting m-carboxy luminol overcame the solubility limitations of its parent compound in neutral solutions [99]. Moreover, incorporating other chemical functionalities could further facilitate coupling with biological probes [100]. These modifications could accelerate the advancement and utilization of luminol systems in various bioanalytical applications, such as ECL-based cellular imaging and the in vivo detection of biomarkers.

ECL Immunoassay

ECL immunoassays (ECLIAs) are one of the most important methods of accurate and sensitive biomarker detection, and thus are widely used for clinical diagnosis and have been successfully implemented in commercialized devices [15, 98]. Labeled immunoassays have witnessed significant advancements, with various label reagents like chromogenic, fluorescent, chemiluminescent (CL), biochemiluminescence (BCL), electrochemical, and ECL being extensively explored [101]. However, challenges persist with certain methods: fluorescent immunoassays are hindered by the fluorescence of proteins themselves, while enzyme-labeled immunoassays face issues related to enzyme instability and the relatively low bioaffinity of large enzyme-labeled antibodies. Additionally, electrochemical immunoassays are constrained by their limited reproducibility and sensitivity.

There are mainly two configurations in ECLIA. In one, immunoreactions are typically conducted on the surface of an electrode and categorized into sandwich, competitive, and direct approaches. Among these methodologies, sandwich ECLIA has been widely favored due to its excellent

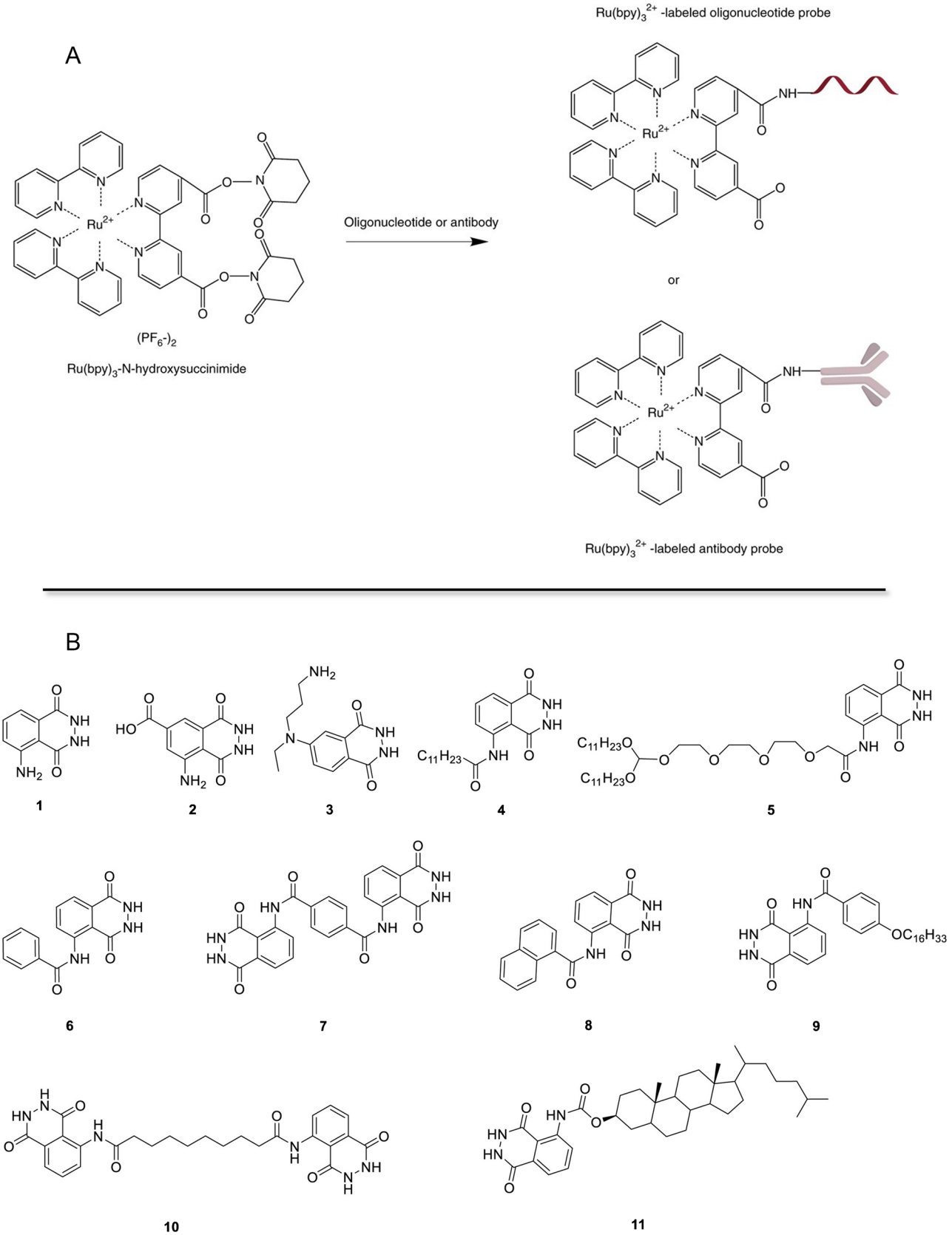

Fig. 11 (**a**) Synthetic route for $Ru(bpy)_3^{2+}$-labeled antibody and $Ru(bpy)_3^{2+}$-labeled oligonucleotide probes through NHS ester. Adapted with permission from [95], Copyright (2014) Nature Journal. (**b**) Structures of luminol and luminol derivatives. Adapted with permission from [97], Copyright (2023) Elsevier

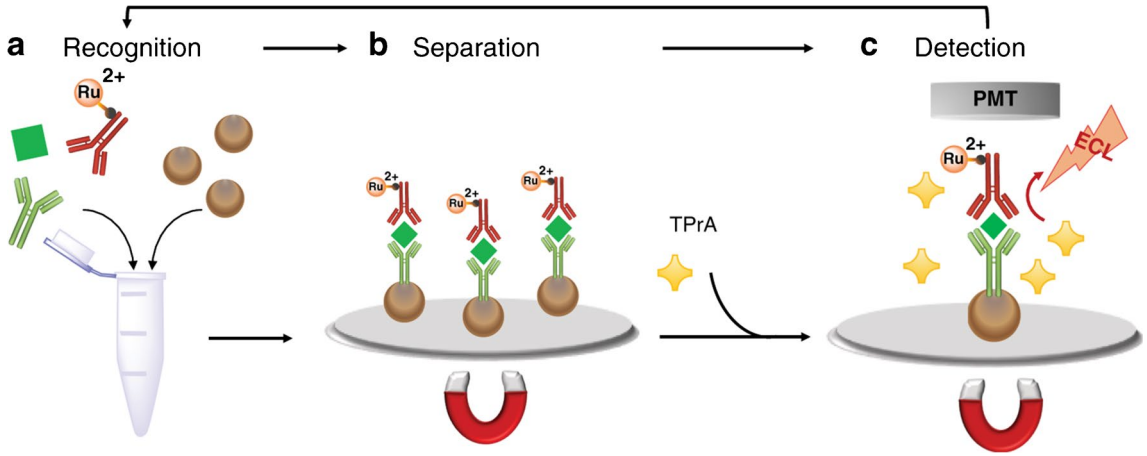

Fig. 12 Schematic representation of the commercial ECLIA system showing (**a**) the recognition phase where the immune sandwich labeled with biotin on one side and the ECL luminophore on the other, is formed and bind to streptavidin-coated microbeads. (**b**) The microbeads separation through a magnetic field and (**c**) the detection of ECL emission by a photomultiplier tube (PMT). Adapted with permission from [15], Copyright (2020) Nature Journals

performance, characterized by high sensitivity, selectivity, and a broad linear range.

In an alternative approach, immunoreactions typically occur in solution rather than on the surface of the working electrode, while ECL measurement takes place on either a bare or chemically modified working electrode in the presence of a coreactant. This approach relies on signal variations arising from steric hindrance, conformational changes, and alterations in the diffusion coefficient induced by the immunoreactions in solution. This type of ECLIA offers simplicity and ease of automation owing to its non-separation process but face the potential adverse effects of complex matrices.

An important ECLIA that is performed on bare working electrodes using immunomagnetic beads is the automated ECL immunoassay system (Elecsys) commercialized by Roche Diagnostic and using $Ru(bpy)_3^{2+}$ and the TPrA system [15]. These immunomagnetic beads, featuring specific capture probes immobilized on their surface (referred to as MBs), play a crucial role in efficiently preconcentrating targets from complex samples [102, 103]. Subsequently, the ECL immunocomplexes formed on the surface of the MBs can be easily separated from the excess ECL probe under through an external magnetic field (Fig. 12).

ECL-DNA biosensing

ECL methods have been employed in nucleic acid assays, leveraging the Watson–Crick base-pairing rule. Typically, the target single-stranded DNA (ss-DNA) is detected using a sandwich hybridization format. In this format, the target ss-DNA first hybridizes with capture probes immobilized on a surface and subsequently hybridizes with ECL probes in solution [104, 105]. Various hybridization strategies have been developed for DNA hybridization ECL biosensing, such as structure switching, target-induced strand displacement, and superhybridization. One straightforward approach is the structure switching format (DNA nanoswitch) [106], where the target single-stranded DNA (ss-DNA) hybridizes with an ECL reagent-labeled hairpin immobilized on the electrode surface leading to a change in the ECL signal [104, 107]. An alternative method for detecting ss-DNA is a label-free one, where the ECL reagent (usually $Ru(phen)_3^{2+}$) interacts with the double-stranded DNA (ds-DNA) [102, 108].

Enzymatic ECL biosensing

Enzymatic ECL biosensing involves an enzyme catalytic reaction with ECL detection, where coreactants serve as either a coproduct or a cofactor of an enzymatic reaction [34] (Fig. 13).

The enzyme is typically immobilized on the electrode surface by physical entrapment or chemical methods forming covalent (e.g., cross-linking with glutaraldehyde or carbodiimide) or non-covalent (e.g., adsorption, affinity) chemical bonds. The immobilization strategy ultimately affects the performance of the biosensor because it can affect the catalytic function and the shelf-life of the enzyme.

Common examples of enzymatic ECL systems include the luminol-H_2O_2 system and the $Ru(bpy)_3^{2+}$-β-nicotinamide adenine dinucleotide (NADH) system as follows:

$$\text{Substrate}_{\text{Red}} + O_2 \longrightarrow \text{Substrate}_{\text{Ox}} + H_2O_2 \quad \text{(oxidase)}$$

$$H_2O_2 + \text{Luminol} \longrightarrow \text{ECL} \quad \text{(applied potential)}$$

$$\text{Substrate}_{\text{Red}} + NAD^+ \longrightarrow \text{Substrate}_{\text{Ox}} + \text{NADH} \quad \text{(dehydrogenase)}$$

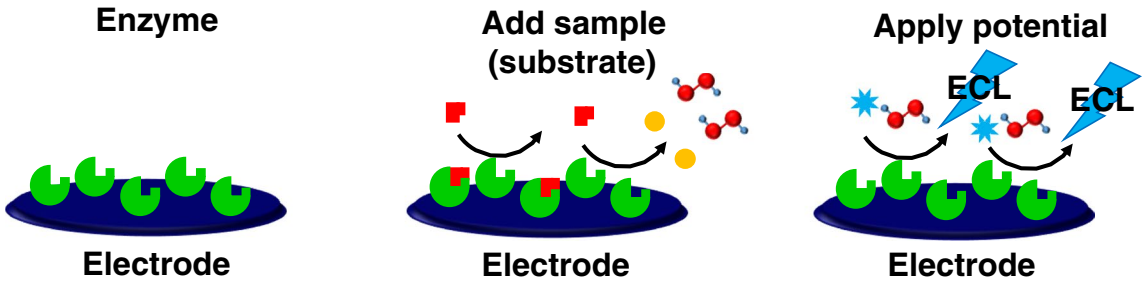

Fig. 13 Schematic representation of an enzymatic ECL biosensor pathway. Adapted with permission from [34], Copyright (2022) Wiley

$$\text{NADH} + Ru(bpy)_3^{2+} \longrightarrow \text{ECL (applied potential)}$$

In the luminol-H_2O_2 system, H_2O_2 is produced through the interaction of dissolved oxygen with enzymatic substrates, catalyzed by the oxidase. Subsequently, H_2O_2 couples with the electrochemical oxidation of luminol, leading to the generation of excited 3-aminophthalic acid. This system has primarily been utilized in quantifying the concentration of enzymatic substrates, including glucose, uric acid, cholesterol, and ethanol, among others. Additionally, it has been applied in ECL immunoassays, using antibodies labeled with glucose oxidase as ECL probes for the identification of biomarkers of interest [109, 110]. However, it is essential to mitigate the chemiluminescence (CL) background arising from the catalytic reaction of metal ions in this system.

In the $Ru(bpy)_3^{2+}$-NADH system, NADH coenzyme acts as a coreactant, generated by NAD+-dependent enzymes such as glucose dehydrogenase, alcohol dehydrogenase, and lactate dehydrogenase using specific substrates. This setup has been employed in quantifying the concentration of enzymatic substrates like glucose, alcohol, and lactate. Nonetheless, these enzymes have drawbacks, including susceptibility to activity loss and high costs.

Conclusion

In conclusion, ECL stands out as a promising avenue for analytical applications. Throughout this review, our aim has been to provide a comprehensive guide to utilize ECL in analytical contexts, elucidating the roles of different components in ECL generation mechanisms and strategies for optimization.

When considering luminophores, inorganic complexes offer distinct advantages in terms of functionalization and homogeneity. On the other hand, organic molecules pose challenges due to issues related to water solubility and conjugation synthesis. Nanomaterials, while holding promise, face challenges in standardization, which impacts the accuracy and reproducibility of results.

Classification of ECL systems based on reaction mechanisms provides insight into optimization strategies. Additionally, the choice of electrode material plays a crucial role in sensitivity, with Pt and Au electrodes preferred in organic solvents, and carbon electrodes offering advantages in aqueous environments. Although, Pt electrode is also used in commercial analyzers.

The recent rise in the utilization of microfluidic paper-based analytical devices reflects a trend toward simplicity and disposability, thereby enhancing accessibility to ECL technology.

Finally, we have discussed new ECL-based protocols that offer opportunities for precise analyte determination through techniques such as immunoassays, enzyme-based assays, and DNA capturing probe systems, leveraging the conjugation of luminophores on specific probes.

In summary, this review sheds light on the multifaceted aspects of ECL in analytical applications, covering fundamental mechanisms as well as emerging protocols. We believe these insights will prove valuable to researchers in the field.

Funding Open access funding provided by Alma Mater Studiorum - Università di Bologna within the CRUI-CARE Agreement. AZ acknowledges the financial support of FSE-REACT-EU, PON Ricerca e Innovazione 2014–2020 DM 1062/202, Cod: 19-G-12549-3. EV acknowledges financial support from Kakenhi Grant-in-Aid (22K14708) from the Japan Society for the Promotion of Science (JSPS). GV and FP would like to thank the MIUR, grant number 20225P4EJC, P2022E5YSK, and 2020CBEYHC (AStraLI). This work was supported by ECLipse project that has received funding from the European Union's Horizon Europe EIC Pathfinder Open programme under Grant Agreement No 101046787.

Declarations

Competing interests The authors declare no competing interests.

References

1. Bard AJ (ed) (2004) Electrogenerated chemiluminescence, 1st ed. CRC Press. https://doi.org/10.1201/9780203027011
2. Liu Z, Qi W, Xu G (2015) Recent advances in electrochemiluminescence. Chem Soc Rev 44:3117–3142. https://doi.org/10.1039/C5CS00086F
3. Richter MM (2004) Electrochemiluminescence (ECL). Chem Rev 104:3003–3036. https://doi.org/10.1021/cr020373d
4. Forster RJ, Bertoncello P, Keyes TE (2009) Electrogenerated chemiluminescence. Annual Rev Anal Chem 2:359–385. https://doi.org/10.1146/annurev-anchem-060908-155305
5. Li L, Chen Y, Zhu JJ (2017) Recent advances in electrochemiluminescence analysis. Anal Chem 89:358–371. https://doi.org/10.1021/ACS.ANALCHEM.6B04675
6. Miao W (2008) Electrogenerated chemiluminescence and its biorelated applications. Chem Rev 108:2506–2553
7. Hong C, Zhang P, Lu K et al (2021) A dual-signal electrochemiluminescence immunosensor for high-sensitivity detection of acute myocardial infarction biomarker. Biosens Bioelectron 194. https://doi.org/10.1016/j.bios.2021.113591
8. Sentic M, Milutinovic M, Kanoufi F et al (2014) Mapping electrogenerated chemiluminescence reactivity in space: mechanistic insight into model systems used in immunoassays. Chem Sci 5:2568–2572. https://doi.org/10.1039/c4sc00312h
9. Pavão e Pavão D, Nascimento Botelho C, Nunes Fernandes R et al (2020) A simple, cost-effective, and environmentally friendly method for determination of ciprofloxacin in drugs and urine samples based on electrogenerated chemiluminescence. Electroanalysis 32:1498–1506. https://doi.org/10.1002/ELAN.201900355
10. Shen Y, Gao X, Lu HJ et al (2023) Electrochemiluminescence-based innovative sensors for monitoring the residual levels of heavy metal ions in environment-related matrices. Coord Chem Rev 476:214927. https://doi.org/10.1016/J.CCR.2022.214927
11. Lenhard JR, Rocklin R, Abruna H et al (1978) Chemically modified electrodes. 11. Predictability of formal potentials of covalently immobilized charge-transfer reagents. J Am Chem Soc 100:5213–5215. https://doi.org/10.1021/JA00484A055/ASSET/JA00484A055.FP.PNG_V03
12. Miao W, Choi JP, Bard AJ (2002) Electrogenerated chemiluminescence 69: the tris(2,2′-bipyridine)ruthenium(II), (Ru(bpy)32+)/tri-n-propylamine (TPrA) system revisited - a new route involving TPrA.+ cation radicals. J Am Chem Soc 124:14478–14485. https://doi.org/10.1021/ja027532v
13. White HS, Bard AJ (1982) Electrogenerated chemiluminescence. 41. Electrogenerated chemiluminescence and chemiluminescence of the Ru(2,2′-bpy)32+-S2O82−system in acetonitrile-water solutions. J Am Chem Soc 104:6891–6895. https://doi.org/10.1021/ja00389a001
14. Tokel NE, Bard AJ (1972) Electrogenerated chemiluminescence. IX. Electrochemistry and emission from systems containing tris(2,2′-bipyridine)ruthenium(II) dichloride. J Am Chem Soc 94:2862–2863. https://doi.org/10.1021/ja00763a056
15. Zanut A, Fiorani A, Canola S et al (2020) Insights into the mechanism of coreactant electrochemiluminescence facilitating enhanced bioanalytical performance. Nat Commun 11. https://doi.org/10.1038/s41467-020-16476-2
16. Glass RS, Faulkner LR (1981) Electrogenerated chemiluminescence from the tris(2,2′-bipyridine)ruthenium(II) system. An example of S-route behavior. J Phys Chem 85:1160–1165. https://doi.org/10.1021/J150609A017/ASSET/J150609A017.FP.PNG_V03
17. McCord P, Bard AJ (1991) Electrogenerated chemiluminescence: Part 54. Electrogenerated chemiluminescence of ruthenium(II) 4,4'-diphenyl-2,2'-bipyridine and ruthenium(II) 4,7-diphenyl-1,10-phenanthroline systems in aqueous and acetonitrile solutions. J Electroanal Chem Interfacial Electrochem 318:91–99. https://doi.org/10.1016/0022-0728(91)85296-2
18. Yuan Y, Han S, Hu L et al (2012) Coreactants of tris(2,2′-bipyridyl)ruthenium(II) Electrogenerated Chemiluminescence. Electrochim Acta 82:484–492. https://doi.org/10.1016/J.ELECTACTA.2012.03.156
19. Quan LM, Stringer BD, Haghighatbin MA et al (2019) Tuning the electrochemiluminescent properties of iridium complexes of N-heterocyclic carbene ligands. Dalton Trans 48:653–663. https://doi.org/10.1039/C8DT04433C
20. Kesarkar S, Mróz W, Penconi M et al (2016) Near-IR emitting iridium(III) complexes with heteroaromatic β-diketonate ancillary ligands for efficient solution-processed OLEDs: structure–property correlations. Angew Chem 128:2764–2768. https://doi.org/10.1002/ange.201509798
21. Stringer BD, Quan LM, Barnard PJ et al (2014) Iridium complexes of N-heterocyclic carbene ligands: investigation into the energetic requirements for efficient electrogenerated chemiluminescence. Organometallics 33:4860–4872. https://doi.org/10.1021/om500076w
22. Marcus RA (1965) On the theory of chemiluminescent electron-transfer reactions. J Chem Phys 43:2654–2657. https://doi.org/10.1063/1.1697190
23. Marcus RA (1960) Exchange reactions and electron transfer reactions including isotopic exchange. Theory of oxidation-reduction reactions involving electron transfer. Part 4. —A statistical-mechanical basis for treating contributions from solvent, ligands, and inert salt. Discuss Faraday Soc 29:21–31. https://doi.org/10.1039/DF9602900021
24. Kerr E, Doeven EH, Wilson DJD et al (2015) Considering the chemical energy requirements of the tri-n-propylamine co-reactant pathways for the judicious design of new electrogenerated chemiluminescence detection systems. Analyst 141:62–69. https://doi.org/10.1039/C5AN01462J
25. Kerr E, Doeven EH, Barbante GJ et al (2015) Annihilation electrogenerated chemiluminescence of mixed metal chelates in solution: modulating emission colour by manipulating the energetics. Chem Sci 6:472–479. https://doi.org/10.1039/c4sc02697g
26. Chen L, Hayne DJ, Doeven EH et al (2019) A conceptual framework for the development of iridium(iii) complex-based electrogenerated chemiluminescence labels. Chem Sci 10:8654–8667. https://doi.org/10.1039/c9sc01391a
27. Miao W, Lu L (2019) Efficient ECL luminophores. RSC Detection Science 2020-January:59–91. https://doi.org/10.1039/9781788015776-00059
28. Yuan Y, Li J, Xu G (2019) Electrochemiluminescence coreactants. RSC Detection Science 2020-January:92–133. https://doi.org/10.1039/9781788015776-00092
29. Kapturkiewicz A (2019) Energetic and kinetic aspects of ECL generation. RSC Detect Sci 2020-January 29–58. https://doi.org/10.1039/9781788015776-00029
30. Villani E, Sakanoue K, Einaga Y et al (2022) Photophysics and electrochemistry of ruthenium complexes for electrogenerated chemiluminescence. J Electroanal Chem 921. https://doi.org/10.1016/j.jelechem.2022.116677
31. Haghighatbin MA, Laird SE, Hogan CF (2018) Electrochemiluminescence of cyclometalated iridium (III) complexes. Curr Opin Electrochem 7:216–223. https://doi.org/10.1016/j.coelec.2018.03.026

32. Kapturkievich
33. Irkham, Rais RR, Ivandini TA et al (2021) Electrogenerated chemiluminescence of luminol mediated by carbonate electrochemical oxidation at a boron-doped diamond. Anal Chem 93:2336–2341. https://doi.org/10.1021/acs.analchem.0c04212
34. Rahmawati I, Einaga Y, Ivandini TA, Fiorani A (2022) Enzymatic biosensors with electrochemiluminescence transduction. ChemElectroChem 9:e202200175. https://doi.org/10.1002/CELC.202200175
35. Fiorani A, Difonzo M, Rizzo F, Valenti G (2022) Versatile electrochemiluminescent organic emitters. Curr Opin Electrochem 34:100998. https://doi.org/10.1016/J.COELEC.2022.100998
36. Kudruk S, Villani E, Polo F et al (2018) Solid state electrochemiluminescence from homogeneous and patterned monolayers of bifunctional spirobifluorene. Chem Commun 54:4999–5002. https://doi.org/10.1039/c8cc02066c
37. Fiorani A, Merino JP, Zanut A et al (2019) Advanced carbon nanomaterials for electrochemiluminescent biosensor applications. Curr Opin Electrochem 16:66–74. https://doi.org/10.1016/j.coelec.2019.04.018
38. Sun H, Zhou P, Su B (2023) Electrochemiluminescence of semiconductor quantum dots and its biosensing applications: a comprehensive review. Biosensors 13:708. https://doi.org/10.3390/BIOS13070708
39. Benoit L, Choi JP (2017) Electrogenerated chemiluminescence of semiconductor nanoparticles and their applications in biosensors. ChemElectroChem 4:1573–1586. https://doi.org/10.1002/CELC.201700219
40. Myung N, Ding Z, Bard AJ (2002) Electrogenerated chemiluminescence of CdSe nanocrystals. Nano Lett 2:1315–1319. https://doi.org/10.1021/nl0257824
41. Ding Z, Quinn BM, Haram SK et al (2002) Electrochemistry and electrogenerated chemiluminescence from silicon nanocrystal quantum dots. Science 296:1293–1297. https://doi.org/10.1126/SCIENCE.1069336/ASSET/B9A22E7A-FD7D-4BDF-BC5D-62F76386EC96/ASSETS/GRAPHIC/SE1920483004.JPEG
42. Bard AJ, Ding Z, Myung N (2005) Electrochemistry and electrogenerated chemiluminescence of semiconductor nanocrystals in solutions and in films. Struct Bond 118:1–57. https://doi.org/10.1007/b137239
43. Hesari M, Ding Z (2017) A grand avenue to au nanocluster electrochemiluminescence. Acc Chem Res 50:218–230. https://doi.org/10.1021/acs.accounts.6b00441
44. Faatz E, Finke A, Josel HP et al (2019) Automated immunoassays for the detection of biomarkers in body fluids. RSC Detection Science 2020-January:443–470. https://doi.org/10.1039/9781788015776-00443
45. Valenti G, Rampazzo E, Biavardi E et al (2015) An electrochemiluminescence-supramolecular approach to sarcosine detection for early diagnosis of prostate cancer. Faraday Discuss 185:299–309. https://doi.org/10.1039/c5fd00096c
46. Rubinstein I, Bard AJ (1981) Electrogenerated Chemiluminescence. 37. Aqueous Ecl Systems Based on Ru(2,2'-bip~ridine),~+ and Oxalate or Organic Acids. J Am Chem SOC 103:512–516
47. Rubinstein I, Martin CR, Bard AJ (1983) Electrogenerated chemiluminescent determination of oxalate. 55:1580–1582
48. Leland JK, Powell MJ (1990) Electrogenerated chemiluminescence: an oxidative-reduction type ECL reaction sequence using Tripropyl Amine. J Electrochem Soc 137:3127–3131. https://doi.org/10.1149/1.2086171/XML
49. Yang H, Leland JK, Yost D, Massey RJ (1994) Electrochemiluminescence: a new diagnostic and research tool. ECL detection technology promises scientists new yardsticks for quantification. Biotechnol (N Y) 12:193–194. https://doi.org/10.1038/NBT0294-193
50. Rebeccani S, Zanut A, Santo CI et al (2022) A guide inside electrochemiluminescent microscopy mechanisms for analytical performance improvement. Anal Chem 94:336–348. https://doi.org/10.1021/acs.analchem.1c05065
51. Fiorani A, Valenti G, Paolucci F, Einaga Y (2023) Electrogenerated chemiluminescence at boron-doped diamond electrodes. Chem Commun 59:7900–7910. https://doi.org/10.1039/d3cc01507f
52. Fiorani A, Han D, Jiang D et al (2020) Spatially resolved electrochemiluminescence through a chemical lens. Chem Sci 11:10496–10500. https://doi.org/10.1039/d0sc04210b
53. Liu X, Shi L, Niu W et al (2007) Environmentally friendly and highly sensitive ruthenium(II) tris(2,2′-bipyridyl) electrochemiluminescent system using 2-(dibutylamino)ethanol as co-reactant. Angewandte Chemie - Int Ed 46:421–424. https://doi.org/10.1002/anie.200603491
54. Kanoufi F, Zu Y, Bard AJ (2001) Homogeneous oxidation of trialkylamines by metal complexes and its impact on electrogenerated chemiluminescence in the trialkylamine/Ru(bpy) 3 2 + system. https://doi.org/10.1021/jp002880
55. Kerr E, Knezevic S, Francis PS et al (2023) Electrochemiluminescence amplification in bead-based assays induced by a freely diffusing iridium(III) complex. ACS Sens 8:933–939. https://doi.org/10.1021/acssensors.2c02697
56. Fracassa A, Santo CI, Kerr E et al (2023) Redox-mediated electrochemiluminescence enhancement for bead-based immunoassay. Chem Sci 15:1150–1158. https://doi.org/10.1039/d3sc06357g
57. Villani E, Valenti G, Marcaccio M et al (2018) Coreactant electrochemiluminescence at nanoporous gold electrodes. Electrochim Acta 277:168–175. https://doi.org/10.1016/j.electacta.2018.04.215
58. Fiorani A, Irkham, Valenti G et al (2018) Electrogenerated chemiluminescence with peroxydisulfate as a coreactant using boron doped diamond electrodes. Anal Chem 90:12959–12963. https://doi.org/10.1021/acs.analchem.8b03622
59. Choi JP, Bard AJ (2005) Electrogenerated chemiluminescence (ECL) 79. Reductive-oxidation ECL of tris(2,2′-bipyridine) ruthenium(II) using hydrogen peroxide as a coreactant in pH 7.5 phosphate buffer solution. Anal Chim Acta 541:141–148. https://doi.org/10.1016/j.aca.2004.11.075
60. Cruz TDS, Akins DL, Birke RL (1976) Chemiluminescence and energy transfer in systems of electrogenerated aromatic anions and benzoyl peroxide. J Am Chem Soc 98:1677–1682. https://doi.org/10.1021/JA00423A007/ASSET/JA00423A007.FP.PNG_V03
61. Zhou P, Fu W, Ding L et al (2023) Toward mechanistic understanding of electrochemiluminescence generation by tris(2,2′-bipyridyl)ruthenium(II) and peroxydisulfate. Electrochim Acta 439:141716. https://doi.org/10.1016/J.ELECTACTA.2022.141716
62. Valenti G, Scarabino S, Goudeau B et al (2017) Single cell Electrochemiluminescence Imaging: from the Proof-of-Concept to Disposable device-based analysis. J Am Chem Soc 139:16830–16837. https://doi.org/10.1021/jacs.7b09260
63. Liu Y, Zhang H, Li B et al (2021) Single biomolecule imaging by electrochemiluminescence. J Am Chem Soc 143:17910–17914. https://doi.org/10.1021/jacs.1c06673
64. Knežević S, Kerr E, Goudeau B et al (2023) Bimodal electrochemiluminescence microscopy of single cells. Anal Chem 95:7372–7378. https://doi.org/10.1021/acs.analchem.3c00869
65. Khan P, Idrees D, Moxley MA et al (2014) Luminol-based chemiluminescent signals: clinical and non-clinical application

and future uses. Appl Biochem Biotechnol 173:333–355. https://doi.org/10.1007/s12010-014-0850-1
66. Hiramoto K, Villani E, Iwama T et al (2020) Recent advances in electrochemiluminescence-based systems for mammalian cell analysis. Micromachines 11:530. https://doi.org/10.3390/MI11050530
67. Sakura S (1992) Electrochemiluminescence of hydrogen peroxide-luminol at a carbon electrode. Anal Chim Acta 262:49–57. https://doi.org/10.1016/0003-2670(92)80007-T
68. Villani E, Inagi S (2021) Mapping the distribution of potential gradient in bipolar electrochemical systems through luminol electrochemiluminescence imaging. Anal Chem 93:8152–8160. https://doi.org/10.1021/acs.analchem.0c05397
69. Villani E, Shida N, Inagi S (2021) Electrogenerated chemiluminescence of luminol on wireless conducting polymer films. Electrochim Acta 389. https://doi.org/10.1016/j.electacta.2021.138718
70. Zhou P, Hu S, Guo W, Su B (2022) Deciphering electrochemiluminescence generation from luminol and hydrogen peroxide by imaging light emitting layer. Fundamental Res 2:682–687. https://doi.org/10.1016/J.FMRE.2021.11.018
71. Fiorani A, Valenti G, Iurlo M et al (2018) Electrogenerated chemiluminescence: a molecular electrochemistry point of view. Curr Opin Electrochem 8:31–38. https://doi.org/10.1016/j.coelec.2017.12.005
72. Valenti G, Fiorani A, Li H et al (2016) Essential role of electrode materials in electrochemiluminescence applications. ChemElectroChem 3:1990–1997. https://doi.org/10.1002/celc.201600602
73. Zu Y, Bard AJ (2000) Electrogenerated chemiluminescence. 66. The role of direct coreactant oxidation in the ruthenium tris(2,2') bipyridyl/tripropylamine system and the effect of halide ions on the emission intensity. Anal Chem 72:3223–3232. https://doi.org/10.1021/ac000199y
74. Zu Y, Bard AJ (2001) Electrogenerated chemiluminescence. 67. Dependence of light emission of the tris(2,2′) bipyridylruthenium(II)/tripropylamine system on electrode surface hydrophobicity. Anal Chem 73:3960–3964. https://doi.org/10.1021/ac010230b
75. Erler K (1998) Elecsys immunoassay systems using electrochemiluminescence detection. Wien Klin Wochenschr 110 Suppl 3:5–10
76. Fiorani A, Eßmann V, Santos CS, Schuhmann W (2020) Enhancing electrogenerated chemiluminescence on platinum electrodes through surface modification. ChemElectroChem 7:1256–1260. https://doi.org/10.1002/celc.202000103
77. Chen Z, Zu Y (2008) Electrogenerated chemiluminescence of the tris(2,2′-bipyridine) ruthenium(II)/tri-n-propylamine (TPrA) system: crucial role of the long lifetime of TPrA + cation radicals suggested by electrode surface effects. J Phys Chem C 112:16663–16667. https://doi.org/10.1021/JP802873E/SUPPL_FILE/JP802873E_SI_001.PDF
78. Valenti G, Zangheri M, Sansaloni SE et al (2015) Transparent carbon nanotube network for efficient electrochemiluminescence devices. Chem---Eur J 21:12640–12645. https://doi.org/10.1002/chem.201501342
79. Watanabe T, Ishikawa R, Hara N et al (2022) Single-layer graphene as a transparent electrode for electrogenerated chemiluminescence biosensing. Electrochem Commun 138. https://doi.org/10.1016/j.elecom.2022.107290
80. Cristarella TC, Chinderle AJ, Hui J, Rodríguez-López J (2015) Single-layer graphene as a stable and transparent electrode for nonaqueous radical annihilation electrogenerated chemiluminescence. Langmuir 31:3999–4007. https://doi.org/10.1021/la5050317
81. Zamolo VA, Valenti G, Venturelli E et al (2012) Highly sensitive electrochemiluminescent nanobiosensor for the detection of palytoxin. ACS Nano 6:7989–7997. https://doi.org/10.1021/nn302573c
82. Villani E, Zhang Y, Chen Z et al (2023) AC-bipolar electrosynthesis and luminol electrochemiluminescence imaging of poly(3,4-ethylenedioxythiophene) and its composite films. ACS Appl Polym Mater 5:6186–6198. https://doi.org/10.1021/acsapm.3c00838
83. Zhou Y, Villani E, Kurioka T et al (2023) Fabrication of luminescent patterns using aggregation-induced emission molecules by an electrolytic micelle disruption approach. Aggregate 4. https://doi.org/10.1002/agt2.202
84. Balmer RS, Brandon JR, Clewes SL et al (2009) Chemical vapour deposition synthetic diamond: materials, technology and applications. J Phys Condens Matter 21. https://doi.org/10.1088/0953-8984/21/36/364221
85. Lagrange JP, Deneuville A, Gheeraert E (1998) Activation energy in low compensated homoepitaxial boron-doped diamond films. Diam Relat Mater 7:1390–1393. https://doi.org/10.1016/S0925-9635(98)00225-8
86. Yang N, Yu S, MacPherson JV et al (2019) Conductive diamond: synthesis, properties, and electrochemical applications. Chem Soc Rev 48:157–204. https://doi.org/10.1039/C7CS00757D
87. Sakanoue K, Fiorani A, Santo CI et al (2022) Boron-doped diamond electrode outperforms the state-of-the-art electrochemiluminescence from microbeads immunoassay. ACS Sens 7:1145–1155. https://doi.org/10.1021/acssensors.2c00156
88. Irkham, Watanabe T, Fiorani A et al (2016) Co-reactant-on-demand ECL: electrogenerated chemiluminescence by the in situ production of S2O82- at boron-doped diamond electrodes. J Am Chem Soc 138:15636–15641. https://doi.org/10.1021/jacs.6b09020
89. Irkham FA, Valenti G et al (2020) Electrogenerated chemiluminescence by in situ production of coreactant hydrogen peroxide in carbonate aqueous solution at a boron-doped diamond electrode. J Am Chem Soc 142:1518–1525. https://doi.org/10.1021/jacs.9b11842
90. Sakanoue K, Fiorani A, Irkham, Einaga Y (2021) Effect of boron-doping level and surface termination in diamond on electrogenerated chemiluminescence. ACS Appl Electron Mater 3:4180–4188. https://doi.org/10.1021/acsaelm.1c00620
91. Gross EM, Durant HE, Hipp KN, Lai RY (2017) Electrochemiluminescence detection in paper-based and other inexpensive microfluidic devices. ChemElectroChem 4:1594–1603. https://doi.org/10.1002/CELC.201700426
92. Delaney JL, Hogan CF, Tian J, Shen W (2011) Electrogenerated chemiluminescence detection in paper-based microfluidic sensors. Anal Chem 83:1300–1306. https://doi.org/10.1021/ac102392t
93. Climent E, Rurack K (2021) Combining electrochemiluminescence detection with aptamer-gated indicator releasing mesoporous nanoparticles enables ppt sensitivity for strip-based rapid tests. Angewandte Chemie - Int Ed 60:26287–26297. https://doi.org/10.1002/anie.202110744
94. Qi H, Zhang C (2020) Electrogenerated chemiluminescence biosensing. Anal Chem 92:524–534. https://doi.org/10.1021/ACS.ANALCHEM.9B03425/ASSET/IMAGES/LARGE/AC9B03425_0004.JPEG
95. Zhou X, Zhu D, Liao Y et al (2014) Synthesis, labeling and bioanalytical applications of a tris(2,2′-bipyridyl)ruthenium(II)-based electrochemiluminescence probe. Nat Protocols 9(5):1146–1159. https://doi.org/10.1038/nprot.2014.060
96. Chen M, Ning Z, Chen K et al (2020) Recent advances of electrochemiluminescent system in bioassay. Journal of Analysis and Testing 4(2):57–75. https://doi.org/10.1007/S41664-020-00136-X

97. Wu K, Zheng Y, Chen R, et al (2023) Advances in electrochemiluminescence luminophores based on small organic molecules for biosensing. Biosens Bioelectron 223:115031. https://doi.org/10.1016/J.BIOS.2022.115031
98. Barhoum A, Altintas Z, Devi KSS, Forster RJ (2023) Electrochemiluminescence biosensors for detection of cancer biomarkers in biofluids: principles, opportunities, and challenges. Nano Today 50:101874. https://doi.org/10.1016/J.NANTOD.2023.101874
99. Mayer M, Takegami S, Neumeier M et al (2018) Electrochemiluminescence bioassays with a water-soluble luminol derivative can outperform fluorescence assays. Angew Chem Int Ed 57:408–411. https://doi.org/10.1002/ANIE.201708630
100. Yang M, Liu C, Qian K et al (2002) Study on the electrochemiluminescence behavior of ABEI and its application in DNA hybridization analysis. Analyst 127:1267–1271. https://doi.org/10.1039/B205783B
101. Muzyka K (2014) Current trends in the development of the electrochemiluminescent immunosensors. Biosens Bioelectron 54:393–407. https://doi.org/10.1016/J.BIOS.2013.11.011
102. Nikolaou P, Valenti G, Paolucci F (2021) Nano-structured materials for the electrochemiluminescence signal enhancement. Electrochim Acta 388:138586. https://doi.org/10.1016/J.ELECTACTA.2021.138586
103. Zanut A, Palomba F, Rossi Scota M et al (2020) Dye-doped silica nanoparticles for enhanced ECL-based immunoassay analytical performance. Angew Chem Int Ed 59:21858–21863. https://doi.org/10.1002/ANIE.202009544
104. Miao W, Bard AJ (2003) Electrogenerated chemiluminescence. 72. Determination of immobilized DNA and C-reactive protein on au(111) electrodes using tris(2,2′ -bipyridyl)ruthenium(II) labels. Anal Chem 75:5825–5834. https://doi.org/10.1021/AC034596V/SUPPL_FILE/AC034596VSI20030805_023034.PDF
105. Du Y, Dong S (2017) Nucleic acid biosensors: recent advances and perspectives. Anal Chem 89:189–215. https://doi.org/10.1021/ACS.ANALCHEM.6B04190/ASSET/IMAGES/LARGE/AC-2016-04190D_0007.JPEG
106. Porchetta A, Ippodrino R, Marini B et al (2018) Programmable nucleic acid nanoswitches for the rapid, single-step detection of antibodies in bodily fluids. J Am Chem Soc 140:947–953. https://doi.org/10.1021/JACS.7B09347/ASSET/IMAGES/JA-2017-09347M_M003.GIF
107. Zanut A, Rossetti M, Marcaccio M et al (2021) DNA-based nanoswitches: insights into electrochemiluminescence signal enhancement. Anal Chem 93:10397–10402. https://doi.org/10.1021/ACS.ANALCHEM.1C01683/ASSET/IMAGES/LARGE/AC1C01683_0004.JPEG
108. Zhang Y, Xu G, Lian G et al (2020) Electrochemiluminescence biosensor for miRNA-21 based on toehold-mediated strand displacement amplification with Ru(phen)32 + loaded DNA nanoclews as signal tags. Biosens Bioelectron 147:111789. https://doi.org/10.1016/J.BIOS.2019.111789
109. Marquette CA, Blum LJ (2006) Applications of the luminol chemiluminescent reaction in analytical chemistry. Anal Bioanal Chem 385:546–554. https://doi.org/10.1007/S00216-006-0439-9/FIGURES/7
110. Li F, Ma W, Liu J et al (2018) Luminol, horseradish peroxidase, and glucose oxidase ternary functionalized graphene oxide for ultrasensitive glucose sensing. Anal Bioanal Chem 410:543–552. https://doi.org/10.1007/S00216-017-0752-5/TABLES/2